Supporting Information

Rotational Symmetry Dication Assembling Ferroelectric, Thermochromic and Circularly Polarized Luminescent Multifunctional Manganese(II) Bromide Hybrid

Jiayi Yuan,[a] Yu Xu,[a] Lu Zhai,*[a] Shan-Shan Hei,[a] Jianyi Huang,[b] Wei-Hua Ning,*[b] Hong-Ling Cai,*[c] and Xiao-Ming Ren*[a]

[a] State Key Laboratory of Materials-Oriented Chemical Engineering and College of Chemistry and Molecular Engineering, Nanjing Tech University, Nanjing 211816, P. R. China

[b] Institute of Functional Nano & Soft Materials (FUNSOM), Joint International Research Laboratory of Carbon-Based Functional Materials and Devices, Soochow University, Suzhou 215123, P. R. China

[c] National Laboratory of Solid-State Microstructures, Collaborative Innovation Center of Advanced Microstructures, School of Physics, Nanjing University, Nanjing 210093, P. R. China

Tel: 86-25-58139476

E-mail:
zhailu@njtech.edu.cn
whning@suda.edu.cn
hlcai@nju.edu.cn
xmren@njtech.edu.cn

Table of Contents

1. Methods and Instrumentation

Reagents and materials

All chemicals and reagents, including 1,4-diazabicyclob[2.2.2]octane (DABCO), manganese (II) bromide tetrahydrate ($MnBr \cdot 4H_2O$, 98%), hydrobromic acid (HBr, 48 wt% in water, Aladdin) and anhydrous methanol (99.7%), methyl bromide, acetone, isopropanol and methanol were purchased from commercial suppliers and used as received.

Synthesis Methods:

Synthesis of [H-Pr-DABCO]Br

The preparation of 1-Propyl-1,4-diazabicyclo[2.2.2]octan-1-ium bromide ([H-Pr-DABCO]Br) is according to the reported method.[1] The obtained product is a colorless, oily liquid.

Synthesis of the single crystal of [H-Pr-DABCO]$MnBr_4$ (1)

Mixture of $MnBr_2 \cdot 4H_2O$ (0.143 g, 0.5 mmol) and [H-Pr-dabco]Br (0.143 g, 0.5 mmol) were dissolved in the solution containing HBr (1 mL) and isopropanol (2 mL). The precursor solution was sealed in a 10 mL Teflonlined autoclave and reacted at 85 ℃ for 24 h, and cooled to room temperature. Subsequently, the solution was volatilized at 50 ℃ for three days and yellow emissive crystals were obtained, which were determined to be [H-Pr-dabco]$MnBr_4$ ($C_9N_2H_{20}MnBr_4$) by single crystal X-ray diffraction. Anal. Calcd. for $C_9N_2H_{20}MnBr_4$: C, 20.36%; H, 3.79%; N, 5.28%; found: C, 20.51%; H, 3.59%; N, 5.25%.

Single crystal X-ray diffraction measurements

Single crystal structure was collected on a Bruker D8 advance diffractometer equipped with a CCD detector by Mo-Kα irradiation (wavelength equal to 0.71073 Å) at 293 K and 438 K. The structures were analyzed by direct methods and refined with full-matrix least-square methods based on F^2 (SHELXL-2014 software package). All non-hydrogen atoms of the structure were refined anisotropically, hydrogen atoms were positioned geometrically and allowed to ride on their parent atoms with constrained thermal parameters. Crystal data and structure refinement parameters are summarized in Table S1. Deposition Numbers 2467490 (for LTP) and 2467491 (for HTP) contains

the supplementary crystallographic data for this paper. These data are provided free of charge by the joint Cambridge Crystallographic Data Centre and Fachinformationszentrum Karlsruhe (http://www.ccdc.cam.ac.uk/structures) Access Structures service.

Powder X-ray diffraction (PXRD)

PXRD of polycrystalline powder was carried out by a MiniFlex600 X-ray diffractometer with Cu Kα (λ = 1.5404 Å) radiation in the 2-theat ranges of 5-50° with a step length of 0.02° to check the phase purity of the as-grown crystals.

Variable-temperature powder X-ray diffraction (PXRD)

Powder X-ray diffraction data were obtained on a Rigaku D/MAX 2000 PC X-ray diffractometer in the temperature range from 298 to 473 K. Diffraction patterns were collected in the 2θ range of 5−50° with a step size of 0.02°.

Thermogravimetric, Differential scanning calorimetry and Dielectric measurements

The thermogravimetric (TG) analysis measurement was performed on a HITACHI STA200 simultaneous thermal analyze at a heating rate of 10°C min^{-1} from room temperature to 800 °C in N_2 flow using an alumina crucible. Differential scanning calorimetry (DSC) measurements were carried out within the specified temperature range at a rate of 20 K min^{-1} using a PerkinElmer Diamond DSC instrument. Dielectric were measured under N_2 atmosphere using a Concept 80 system (Novocontrol, Germany) from 150 K to 400 K with the frequency of 10^3–10^7 Hz. The powder sample was pressed into a pellet with a diameter of 7 mm. And then the silver paste was evenly smeared on both sides to make a capacitor.

Second-harmonic generation (SHG) .

The SHG response was measured, using the Kurtz–Perry method with a home-built scanning microscope using an Nd:YAG laser (wavelength of 1064 nm, input pulse power of 400 mV) in reflection geometry. The numerical values of the nonlinear optical coefficients for SHG have been determined by comparison with a KH_2PO4 (KDP) reference. The test samples were polycrystalline powder.

Polarization-Electric Field (P-E) Hysteresis Loops

P-E hysteresis loops measurements were performed on a powder-pressed pellet sample by using the so-called double-wave method. The Positive Up Negative Down (PUND) ferroelectric tests were got on a Precision LC ferroelectric analyzer (Radiant Technology Product, USA). The ferroelectric hysteresis loop was got by TF Analyzer 2000E. The single crystal selected to measure the dielectric hysteresis loop on a ferroelectric tester (Radient Technology), with electrodes made of Cu wire with an ~150 μm diameter covered by Ag-conducting glue on the approximate crystallographic face (001), respectively.

Optical Measurements

The UV-vis diffuse reflectance spectra were measured using a UV-vis absorption spectrophotometer (PerkinElmer, Lambda 1050) in the wavelength range of 200–800 nm. The PL spectra, PLE spectra, time-resolved PL, and photoluminescence quantum yield (PLQY) of the sample were measured on an Edinburgh Instruments FLS1000 fluorescence spectrometer at room temperature. The temperature-dependent PL spectra were carried out using a fluorescence spectrometer (PL-TCSPC) in the excitation wavelength of 365 nm at 80 to 300 K. The time-resolved photoluminescence (TRPL) measurement was performed using a fluorescence spectrometer (PL-TCSPC). The PLQY was measured using an absolute PL measurement system (C13534-11, Hamamatsu) and the excitation wavelength was 365 nm.

Circular Dichroism Spectra (CD)

The CD spectra were collected using a CD spectrometer (J-1500, JASCO) at room temperature. The samples for CD measurement were prepared by uniformly grinding the crystals with KBr into fine powder and then pressing into pellets, which were employed as the matrix for performing solid-state CD measurements.

Circularly polarized photoluminescence spectroscopy (CPL)

CPL measurements of single crystals of **1** were performed on a JASCO CPL-300 spectrometer at λ_{ex} = 365 nm. A single crystal was placed in the optical path so that the optical path was perpendicular to the smooth crystal plane. The excitation wavelength employed was 365 nm. All measurements were performed at room temperature.

Hirshfeld surface analysis

Various types of intermolecular interactions are quantified through Hirshfeld surface analysis using the CrystalExplorer21.5 software. On Hirshfeld surfaces mapped with d_{norm}, points shorter than the van der Waals distance are labeled red, and points equal to or longer than the van der Waals distance are labeled white and blue, which intuitively provides a perspective for assessing intermolecular interactions.

Calculations of Tanabe-Sugano (T-S) Matrices. The crystal field Dq, Racah parameter B and correction parameter α were obtained using the modified energy terms derived by Tanabe and Sugano as follows:

$^6S \rightarrow {}^4A_1$; $^4E(^4G) = 10B + 5C + 20\alpha$

$^6S \rightarrow {}^4E(^4D) = 17B + 5C + 6\alpha$

$^6S \rightarrow {}^4T_2(^4D) = 13B + 5C + 8\alpha$

$^6S \rightarrow {}^4T_2(^4G) = -10Dq + 18B + 6C - (26B^2/10Dq) + 22\alpha$

Calculated results: 10Dq = 6173, B = 21, C = 5811 and α = –324

Characterization

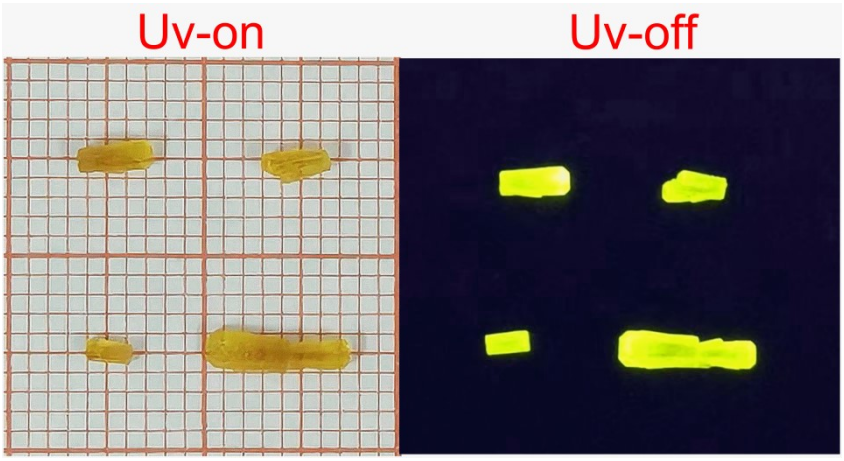

Figure S1. Photographs of single crystals of **1** taken under ambient light and 365 nm ultraviolet light.

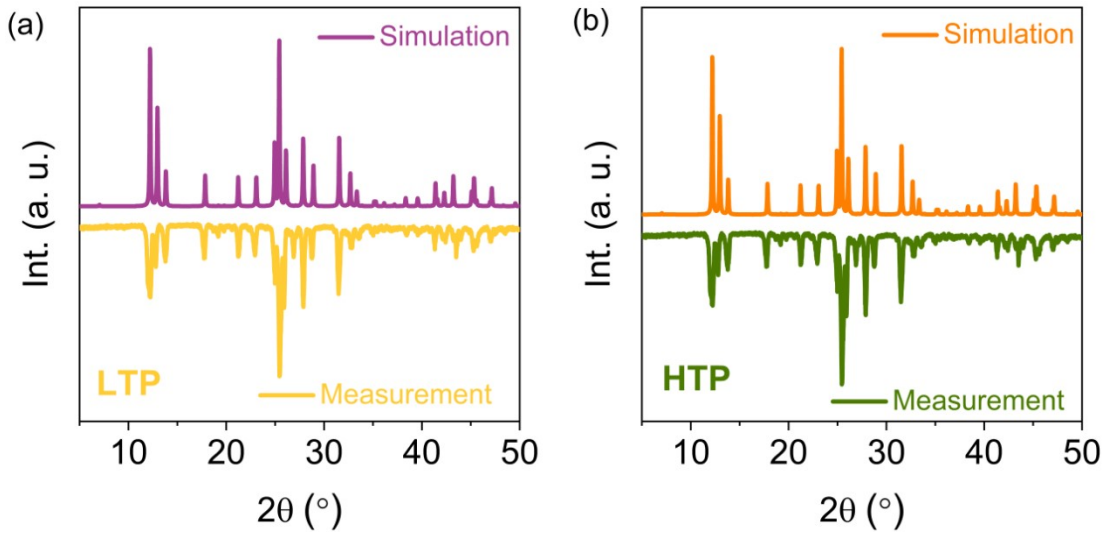

Figure S2. The experimental PXRD patterns and simulated ones based on the single crystal structure of **1** at (a) 293 K (LTP) and (b) 438 K (HTP).

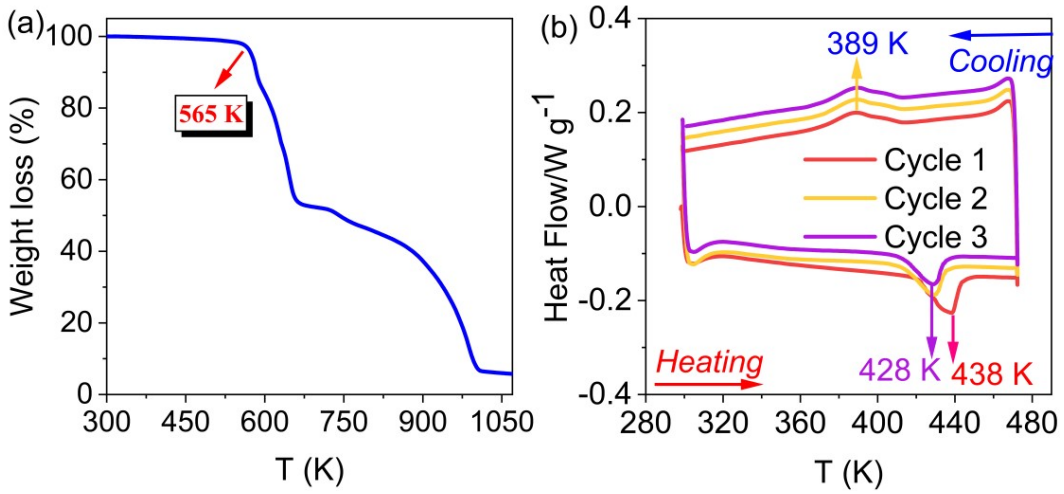

Figure S3. (a) TG curve of **1** in the temperature range from 30 to 800 °C in N_2 flow. (b) DSC curves in three heating-cooling cycles.

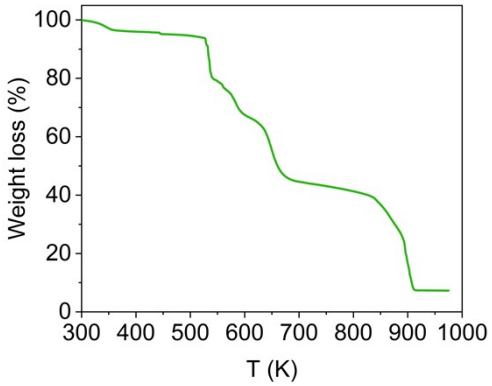

Figure S4. The thermal stability of **1** in air.

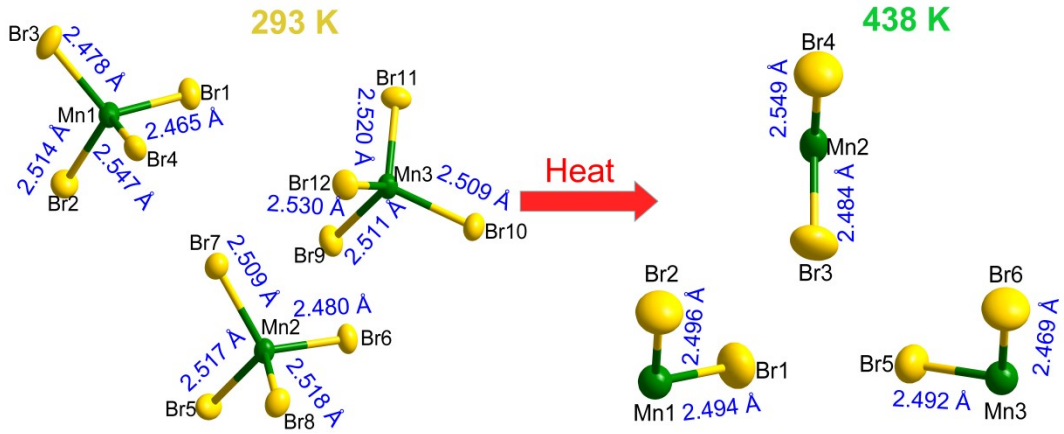

Figure S5. Comparison of Mn-Br bond lengths in the crystal structures of LTP and HTP.

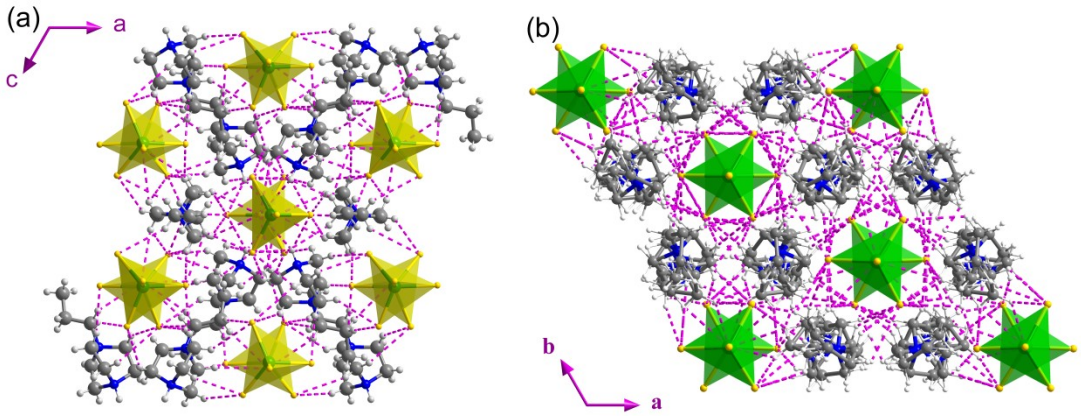

Figure S6. Schematic illustration for the hydrogen bonds using dot lines in (a) LTP and (b) HTP.

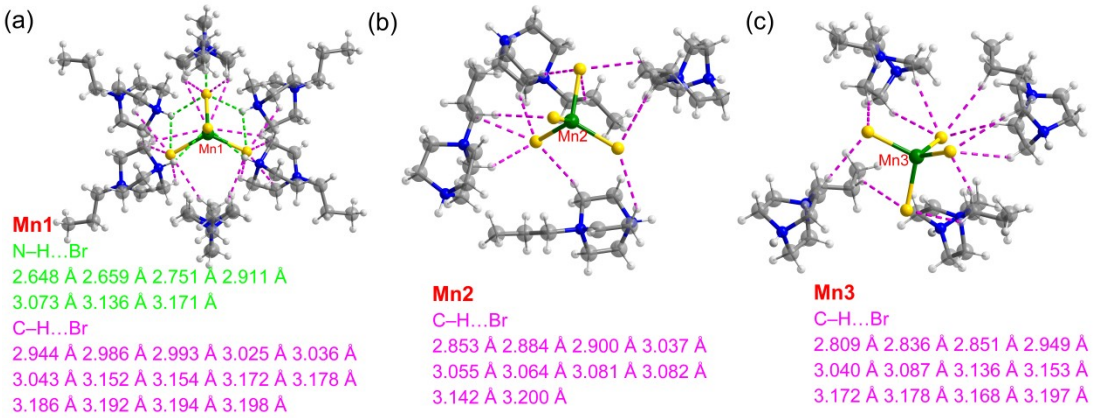

Figure S7. The local hydrogen bonding interactions around the $[MnBr_4]^{2-}$ for (a) Mn1 (b) Mn2 and (c) Mn3 tetrahedron in LTP, respectively. The green dotted lines represent the N–H…Br hydrogen bonds while the pink dotted lines represent the C–H…Br hydrogen bonds between organic cations and inorganic frameworks.

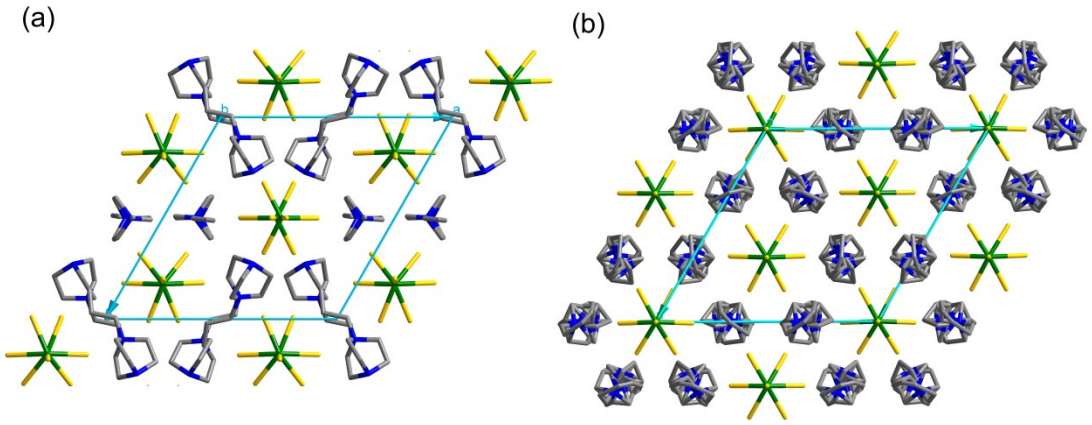

Figure S8. The Mn^{2+} ions within a lattice reorganized from (a) a non-collinear arrangement (LTP) to (b) a collinear arrangement (HTP).

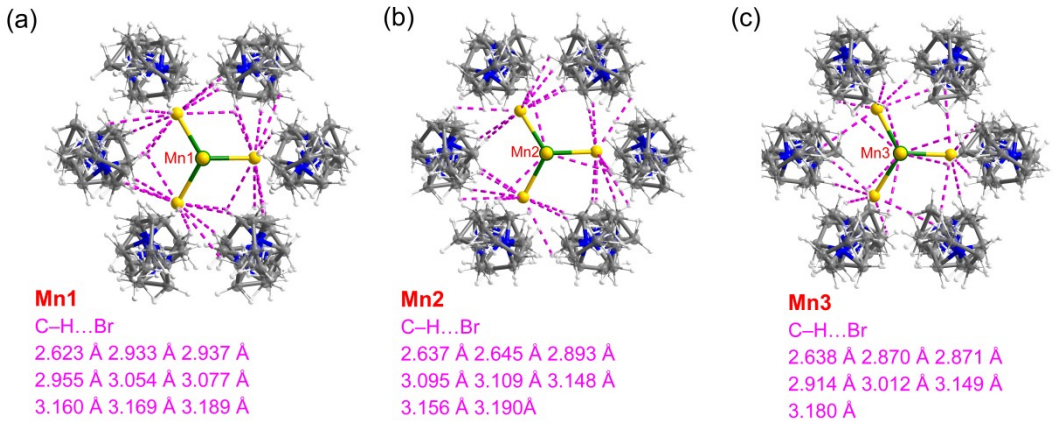

Figure S9. The hydrogen bonding interactions around the $[MnBr_4]^{2-}$ for (a) Mn1 (b) Mn2 and (c) Mn3 tetrahedron in HTP, respectively. The pink dotted lines represent the C–H…Br hydrogen bonds between organic cations and inorganic frameworks.

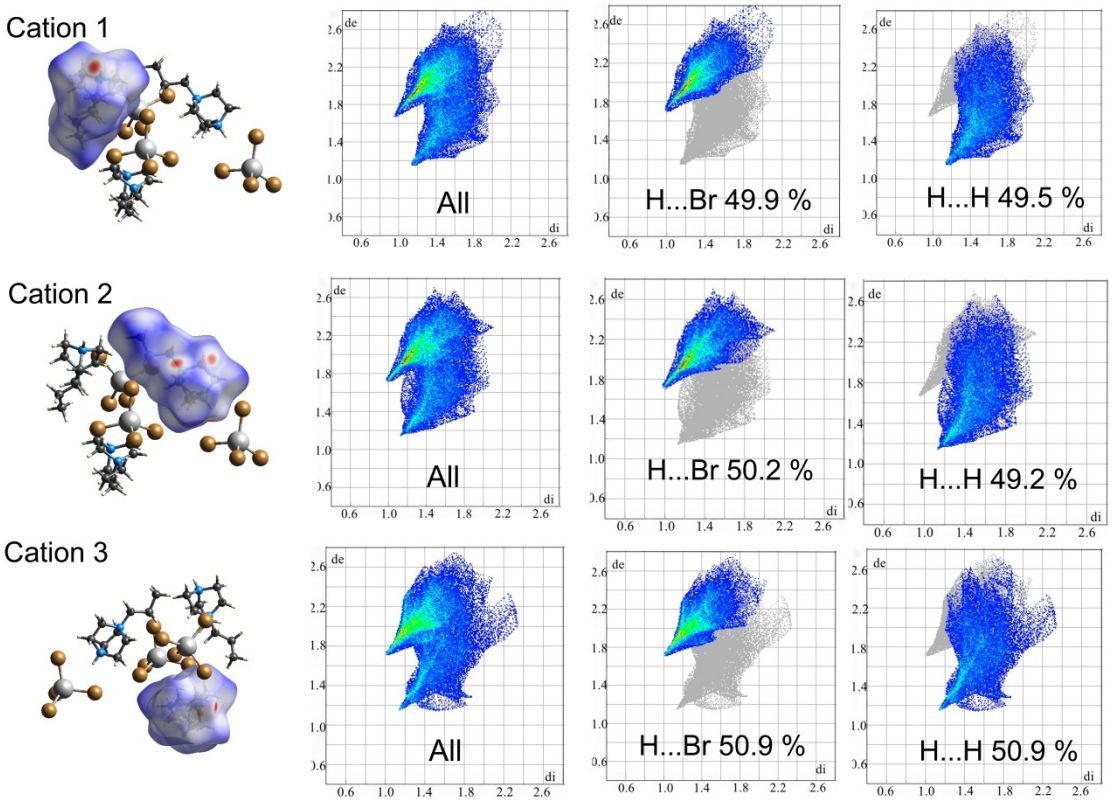

Figure S10. Hirshfeld surface and 2D fingerprint of the cations of in the asymmetric unit of LTP.

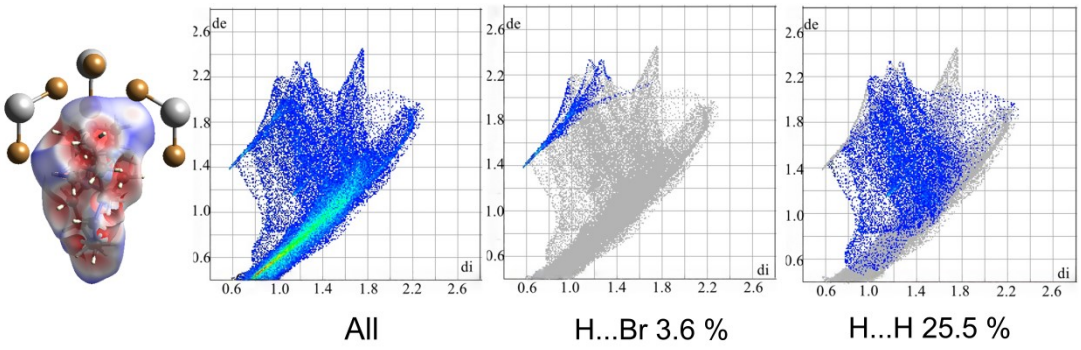

Figure S11. Hirshfeld surface and 2D fingerprint of the cations of in the asymmetric unit of HTP.

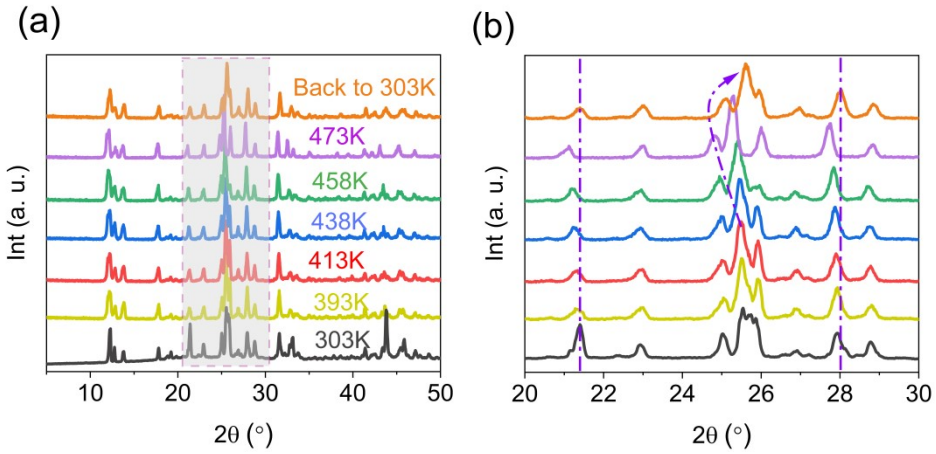

Figure S12. Variable-temperature PXRD patterns of (a) **1** within the 2θ range of 5–50° and (b) within a special range where the obvious changes occur.

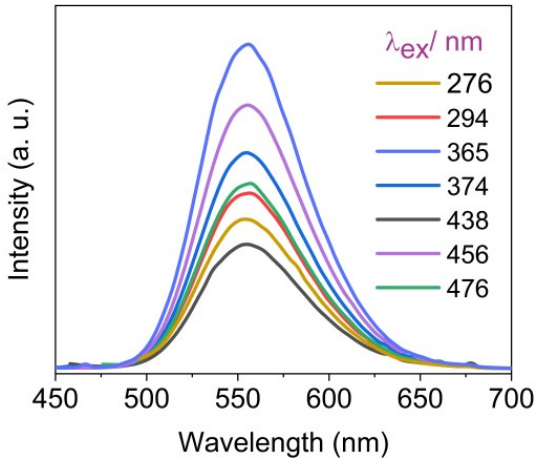

Figure S13. Excitation-dependent PL spectra of **1** at 298 K.

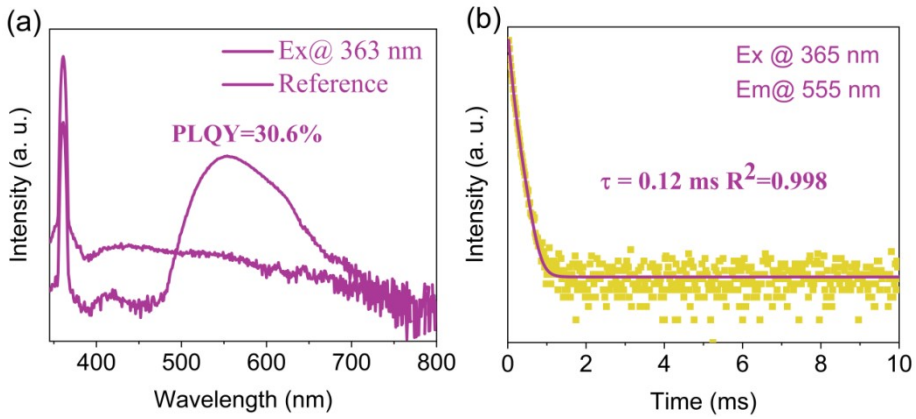

Figure S14. (a) The PLQY measurement of **1** at room temperature upon 365 nm UV excitation (b) the decay lifetime monitored at 555 nm.

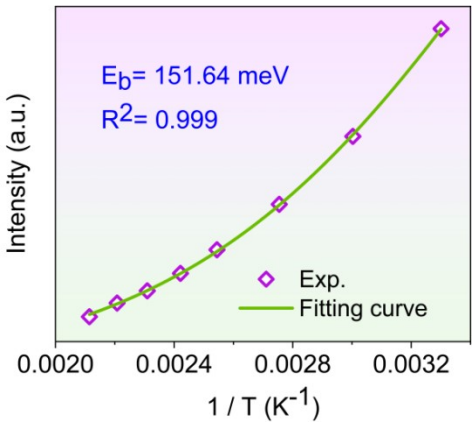

Figure S15. The fitted curve of PL intensity to temperature using the Arrhenius equation.

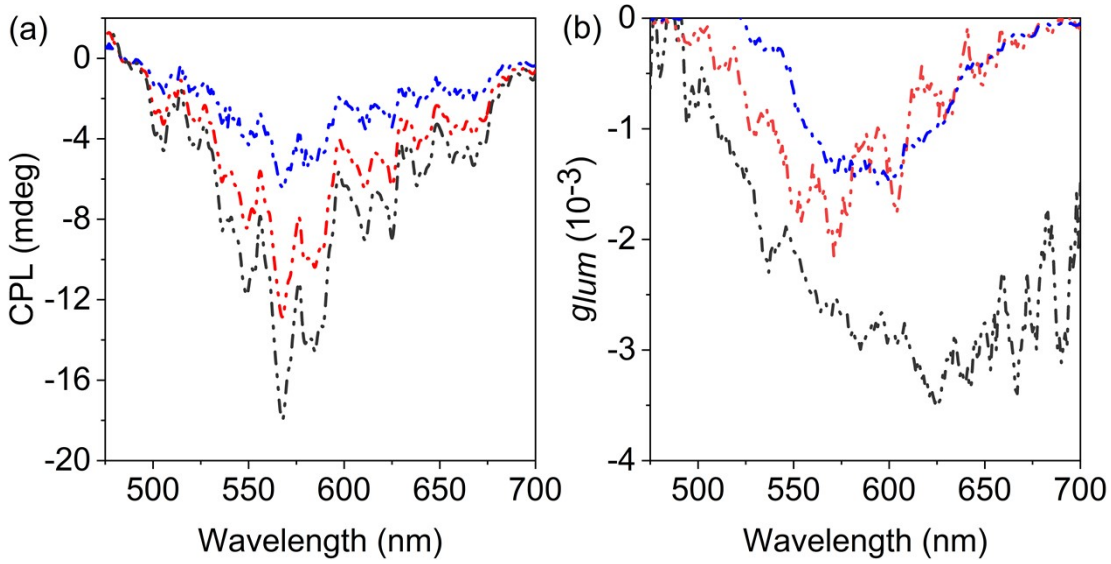

Figure S16. (a) CPL and (b) g_{lum} spectra of **1** with different angle measurements.

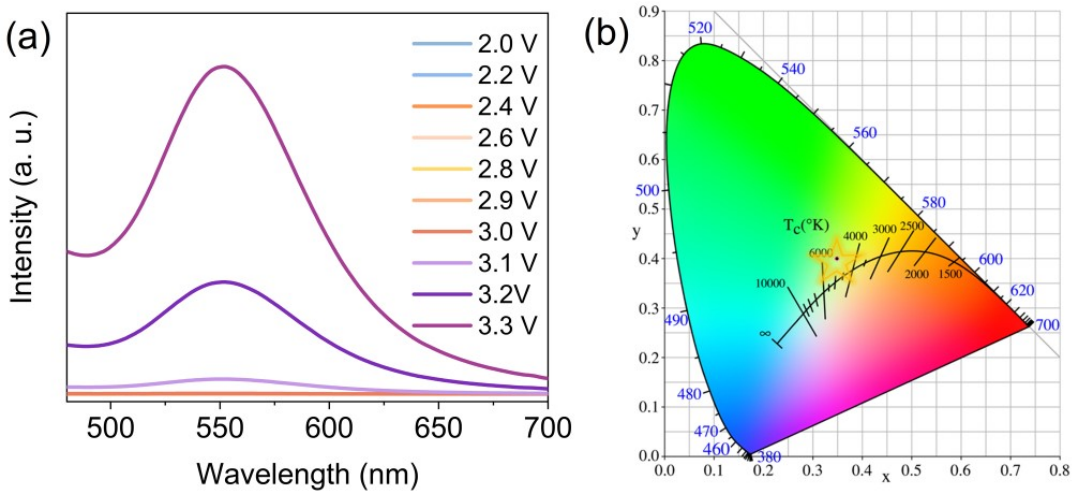

Figure S17. (a) The electroluminescence spectra of the LED at different voltages. (b) CIE diagram of the LED constituted of **1**.

Point Charge Calculation on Saturated Polarization

According to the crystallographic data of **1** at LTP and HTP phase, we select a unit cell and assume that the centers of the positive charges of the cations are located on the N, Mn atoms, and the negative charges of the anions are located on the Br atoms, respectively.

Atoms (Count)	Center coordination
	293 K
Mn^{2+}(6)	(0.51013, 0.57607, 0.35427)
N^{+}(12)	(0.57263, 0.46473, 0.50010)
Br^{-}(24)	(-0.48930, -0.60033, -0.41677)

Along *c*-axis:

$$P_s = \lim \frac{1}{V} \sum q_i r_i$$

$= (q_N r_N + q_{Mn} r_{Mn} + q_{Br} r_{Br}) / V$

$= [(12 \times e \times 0.35427) + (2 \times 6 \times e \times 0.50010) + (-24 \times e \times 0.41677] \times c / V$

$= [0.24996 \times 1.6 \times 10^{-19} \times 14.316 \times 10^{-10}\ C\ m] / (2424.0 \times 10^{-30}\ m^3)$

$= 0.02362\ C\ m^{-2}$

$|P_s| = 0.02362\ C\ m^{-2} = 23.62\ \mu C\ cm^{-2}$

3. Supporting Tables

Table S1. The crystallographic and structure refinement data for LTP and HTP

Identification code	**LTP**	**HTP**
Chemical formula	$C_9H_{19}N_2MnBr_4$	$C_9H_{19}N_2MnBr_4$
CCDC number	2467490	2467491
Formula weight	529.84	529.84
Tempetature / K	293.00	438.15
Crystal system	Monoclinicc	Rrigonal
Space group	$P2_1$	$P3c_1$
a / Å	14.2814(11)	14.4907(16)
b / Å	13.6741(9)	14.4907(16)
c / Å	14.3160(16)	13.6423(18)
α / °	90	90
β / °	90	90
γ / °	120	120
V (Å^3) / Z	2424.0(4)/6	2480.8(6)/6
F(000)	1512	1512
θ range for data collection /°	2.84 to 23.39	2.811 to 26.369
Index range	-16≤ h ≤17 -15≤ k ≤16 -17≤ l ≤17	-16≤ h ≤18 -18≤ h ≤16 -18≤ h ≤17
Refl. collected/unique	17852 / 22445	18760
Goodness-of-fit on F^2	1.037	1.053
Final *R* indices [I>2σ(I)]	R_1 = 0.0929, wR_2 = 0.2259	R_1 = 0.0942, wR_2 = 0.2533
R indices(all data)	R_1 = 0.1150, wR_2=0.2408	R_1 = 0.1833, wR_2 = 0.3099
Flack parameter	0.006(15)	0.19(11)

Table S2. Selected bond distances (Å) and bond angles (°) for LTP and HTP

	Bond length (Å)		Bond angle (°)	
LPT	Mn1-Br1	2.465(9)	Br3-Mn1-Br4	104.1(3)
	Mn1-Br2	2.514(8)	Br3-Mn1-Br2	108.8(3)
	Mn1-Br3	2.478(8)	Br1-Mn1-Br4	104.5(3)
	Mn1-Br4	2.547(9)	Br1-Mn1-Br3	118.8(4)
	Mn2-Br5	2.517(8)	Br1-Mn1-Br2	108.1(3)
	Mn2-Br6	2.480(8)	Br2-Mn1-Br4	112.5(3)
	Mn2-Br7	2.509(8)	Br7-Mn2-Br8	115.6(3)
	Mn2-Br8	2.518(8)	Br7-Mn2-Br5	104.4(3)
	Mn3-Br9	2.511(9)	Br6-Mn2-Br8	108.7(3)
	Mn3-Br10	2.509(8)	Br6-Mn2-Br7	112.7(3)
	Mn3-Br11	2.520(8)	Br6-Mn2-Br5	109.1(3)
	Mn3-Br12	2.530(8)	Br5-Mn2-Br8	105.9(3)
			Br11-Mn3-Br12	115.5(3)
			Br10-Mn3-Br11	108.5(3)
			Br10-Mn3-Br12	110.3(3)
			Br10-Mn3-Br9	110.8(3)
			Br9-Mn3-Br11	106.4(3)
			Br9-Mn3-Br12	105.3(3)
HTP	Mn1-Br1	2.494(4)	Br1-Mn1-Br1	109.6(2)
	Mn1-Br2	2.496(10)	Br1-Mn1-Br2	109.3(2)
	Mn2-Br3	2.484(4)	Br3-Mn2-Br3	113.0(2)
	Mn2-Br4	2.549(12)	Br3-Mn2-Br4	105.7(2)
	Mn3-Br5	2.492(4)	Br5-Mn3-Br5	110.5(2)
	Mn3-Br6	2.469(10)	Br6-Mn1-Br5	108.4(2)

Table S3. Details of hydrogen and halogen bonds of LTP

Hydrogen bonding	D-A (Å)	Hydrogen bonding	D-H...A ()
C2 -H…Br8	3.200	C7 -H…Br7	3.053
C7 -H…Br1	3.198	C9 -H…Br2	3.043
C9 -H…Br9	3.197	C7 -H…Br12	3.040
C5 -H…Br2	3.194	C2 -H…Br5	3.037
C7 -H…Br2	3.192	C2 -H…Br5	3.036
C3 -H…Br12	3.187	C9 -H…Br3	3.025
C5 -H…Br3	3.186	C9 -H…Br9	3.019
C7 -H…Br2	3.178	C2-H…Br3	2.993
C2 -H…Br6	3.175	C7-H…Br1	2.986
C9 -H…Br3	3.172	C5-H…Br12	2.978
N2 -H…Br2	3.171	C2-H…Br12	2.961
C3 -H…Br9	3.168	C5-H…Br12	2.949
C9 -H…Br5	3.156	C2-H…Br3	2.911
C5 -H…Br1	3.154	C3-H…Br6	2.900
C5 -H…Br10	3.153	N2-H…Br3	2.911
C9 -H…Br12	3.152	C4-H…Br8	2.884
C4 -H…Br6	3.145	C6-H…Br10	2.857
C3 -H…Br5	3.142	C4-H…Br8	2.853
N4 -H…Br10	3.136	C3 -H…Br10	2.851
C7 -H…Br5	3.121	C2 -H…Br7	2.844
C5 -H…Br7	3.102	C8 -H…Br11	2.836
C2 -H…Br10	3.087	C6 -H…Br11	2.827
C9 -H…Br6	3.082	C4 -H…Br11	2.809
C6 -H…Br8	3.081	N2 -H…Br4	2.751
N2 -H…Br1	3.073	N2 -H…Br4	2.659
C6 -H…Br5	3.064	N2 -H…Br4	2.648
C3 -H…Br7	3.055		

Table S4. Details of hydrogen and halogen bonds of HTP

Hydrogen bonding	D-A (Å)	Hydrogen bonding	D-H...A ()
C1 -H…Br4	3.190	C8 -H…Br1	3.077
C6 -H…Br1	3.189	C3 -H…Br1	3.054
C2 -H…Br6	3.180	C1 -H…Br5	3.012
C8 -H…Br1	3.169	C2 -H…Br1	2.955
C2 -H…Br1	3.160	C4 -H…Br1	2.937
C3 -H…Br1	3.156	C6 -H…Br1	2.933
C6 -H…Br5	3.149	C6 -H…Br3	2.893
C3 -H…Br2	3.148	C4 -H…Br5	2.871
C7 -H…Br3	3.109	C3 -H…Br5	2.870
C8 -H…Br3	3.095	C7 -H…Br5	2.638

Table S5. Bond length distortion and bond angle variance of $MnBr_4$ units of LTP and HTP.

(Δd: calculated bond-length distortion degrees, σ^2 : bond angle distortion)

Crystal	Units	Δd (10^{-5})	σ^2	Crystal	Units	Δd (10^{-5})	σ^2
LTP	Mn1	16.48	28.95	HTP	Mn1	0.016	0.027
	Mn2	3.78	14.95		Mn2	16.68	16.00
	Mn3	1.09	13.31		Mn3	0.64	1.32
	average	7.12	19.07		average	5.78	5.78

Table S6. Comparison of g_{lum}, curie temperature (T_c), PLQY, SHG intensity and saturation polarization (P_s) values inside this work with other multifunctional materials in literatures (black) and this work (red)

Compounds	g_{lum} (10^{-3})	T_c (K)	PLQY (%)	SHG intensity (vs KDP)	P_s (μCcm^{-2})
OAO-$MnCl_4$ and OAO- $MnBr_4$ [2]	/	363	/	/	0.51/0.59
(*S*-CTA)$_2$$CuCl_4$ and (*R*-CTA)$_2$$CuCl_4$ [3]	/	417/420	/	1/6-1/4	/
(AMP)$_2$$SbBr_5$[4]	/	327	/	1.3	11.28
[TMIm][$MnCl_4$][5]		443/429	27		/
CystaH_2[$CuCl_4$][6]	/	384	/	/	1.65
(pyrrolidinium)$MnBr_3$[7]	/	219	28.5	/	5.7
R/*S*-3-(fluoropyrrolidinium)$MnBr_3$[8]	6.1	273	28.13/32	/	4.5/4.8
[MeHdabco]RbI_3[9]	/	430	17.17	/	6.8
(IYA)$SbBr_5$[10]	/	392	/	0.7	2.3
[DMe-DABCO]$CuCl_4$[11]	/	413	/	/	0.53
[DFPIP]$_4$$AgBiI_8$[12]	/	422	/	1	10.5
[$C_6H_{16}N_2$]PbI_4[13]	/	355	/	1.7	15.6
([$C_8H_{11}ClN$]$_2$$PbI_4$)[14]	/	483	/	0.5	13.96
[$Me_3NCH_2CH_2OH$]$CdCl_3$[15]	/	360/400	/	/	17.1
1 (This work)	4.8	428	30.6	0.88	21.5

4. References

1. V. I. Kovalenko, A. A. Akhmadiyarov, A. E. Vandyukov, A. R. Khamatgalimov, J. *Mol. Struct*. 2012, **1028**, 134.
2. W. Zhang, S. Jiao, M. Zhao, C. Xu, Z. Yang, D. Li, Z. Tang, Y. Lu, H.-L. Cai, X. S. Wu, *J. Phys. Chem. C.,* 2023, **127**, 17261.
3. R.-G. Xiong, S-Q. Lu, Z.-X. Zhang, H. Cheng, P.-F. Li, W.-Q. Liao, *Angew. Chem. Int. Ed.,* 2020, **59**, 9574.
4. B. Zhuang, L. Pan, Z.-L. Li, J.-Y. Liu, Z.-X. Zhang, K. Ding, Y. Zhang, Z. Liu, D.-W. Fu, *ACS Materials Lett*., 2025, **7**, 1540.
5. W.-L. Yang, X. Yan, M. Wang, H. Yuan, Y.-Y. Tang, Y. Qin, X.-J. Song, *Inorg. Chem. Front*., 2024, **11**, 6874.
6. W.-F. Deng, Y.-X. Li, Y.-X. Zhao, J.-S. Hu, Z.-S. Yao, J. Tao, *J. Am. Chem. Soc*.,

2023, **145**, 5545.

7. Y. Zhang, W.-Q. Liao, D.-W. Fu, H.-Y. Ye, C.-M. Liu, Z.-N. Chen, R.-G. Xiong, *Adv. Mater*., 2015, **27**, 3942.

8. J.-X. Gao, W.-Y. Zhang, Z.-G. Wu, Y.-X. Zheng, D.-W. Fu, *J. Am. Chem. Soc*., 2020, **142**, 10, 4756.

9. W.-Y. Zhang, Y.-Y. Tang, P.-F. Li, P.-P. Shi, W.-Q. Liao, D.-W. Fu, H.-Y. Ye, Y. Zhang, R.-G. Xiong, *J. Am. Chem. Soc*., 2017, **139**, 10897.

10. P. Chen, Z. Zhou, X. Li, S. Jiao, Y. Qin, Y. Shen, H.-L. Cai, X. S. Wu, *Inorg. Chem*., 2025, **64**, 16487.

11. J.-C. Liu, W.-Q. Liao, P.-F. Li, Y.-Y. Tang, X.-G. Chen, X.-J. Song, H.-Y. Zhang, Y. Zhang, Y.-M. You, R.-G. Xiong, *Angew. Chem. Int. Ed*., 2020, **59**, 3495.

12. C.-F. Wang, H. Li, M.-G. Li, Y.Cui, X. Song, Q.-W. Wang, J.-Y. Jiang, M.-M. Hua, Q. Xu, K. Zhao, H.-Y. Ye, Y. Zhang, *Adv. Funct. Mater*., 2021, **31**, 2009457.

13. W.-C. Qiao, H. Qiao, X. L. Wang, H. Xu, F. Xu, Z. Sun, H. Gao, Y.-F. Yao, *Small* 2024, **20**, 2310529.

14. C.-K. Yang, W.-N. Chen, Y.-T. Ding, J. Wang, Y. Rao, W.-Q. Liao, Y.-Y. Tang, P.-F. Li, Z.-X. Wang, R.-G. Xiong, *Adv. Mater*., 2019, **31**, 1808088.

15. S. Deswal, S. K. Singh, R. Pandey, P. Nasa, D. Kabra, B. Praveenkumar, S. Ogale, R. Boomishankar, *Chem. Mater*., 2020, **32**, 19, 8333.